JOURNAL OF MATERIALS SCIENCE 28 (1993) 6785–6798

Effect of melt, solidification and heat-treatment processing parameters on the properties of Al–Si–Mg/SiC(p) composites

A. M. SAMUEL, H. LIU, F. H. SAMUEL
Département des Sciences Appliquées, Université du Québec à Chicoutimi, Chicoutimi, Québec, Canada G7H 2B1

With the recent renovations in casting technology and foundry procedures, Al–Si–Mg alloys reinforced with SiC particulates are being increasingly employed in automotive and aerospace applications. The SiC reinforcement particles influence the solidification process in various ways, affecting the fluidity and castability of these composites.

This articles reviews the results of an extensive study carried out on different aspects of Al–Si–Mg/$SiC_{(p)}$-type metal-matrix composites containing 7 or 10 wt% Si, reinforced with either 10 or 20 vol% SiC particulates. Aspects investigated include the castability and soundness in terms of melt fluidity, the effect of the solidification rate and of inclusions on the mechanical properties, and optimization of the heat-treatment parameters with regard to these properties. The influence of the processing parameters on the mechanical properties was determined by monitoring the microstructural changes taking place during the various stages of processing, by measurements of the dendrite arm spacing, porosity and SiC-particle content and distribution in the castings obtained, as well as the amount of oxide inclusions and other harmful reaction products such as Al_4C_3 present therein. The effect of employing the fluxing procedure commonly used in Al–Si–Mg alloys on the mechanical properties of one of the four composites studied is also reported.

1. Introduction

There have been many pioneering efforts over the last forty years in the development of metal-matrix composites (MMCs) as new engineering materials; they have improved properties, and lightweight characteristics and competitive costs compared to traditional materials. Following recent advances in casting technology and the use of melt-stirring devices by foundries, Al–Si–Mg alloys reinforced with SiC powders or short alumina fibres are being employed in the production of castings targeted for automotive and aerospace applications [1, 2]. To produce these composites, both solid-phase and liquid-phase processing methods have been used; the latter have the advantage that the fluidity of the metal allows for the use of a wide range of reinforcements and the capability of producing near-net-shaped castings.

In the particular case of particle-reinforced composites, the reinforcement particles are found to influence the solidification process in various ways – their settling in the melt, chemical reactions with the matrix, as well as the particle pushing that occurs by the impingement of the solidification growth front on these particles. In addition, the particles can also act as nucleation sites under favourable conditions [3]. The fluidity and castability of these composites is thus affected by the particles in one or more of these ways.

Composite quality, or more particularly, cleanliness of the molten composite prior to casting is chiefly determined by the hydrogen and inclusion content of the melt. The deleterious effect of both hydrogen and inclusions on the quality of the cast product is amply recorded in the literature [4, 5]. While removal of hydrogen is accomplished by various melt procedures (such as degassing or fluxing) inclusions can be removed by the use of filtration [6] and a properly designed gating system [7]. Filtration allows for removal of non-metallic and intermetallic inclusions whose presence in the melt can otherwise reduce the melt fluidity and the mechanical properties and increase the internal porosity of the casting, giving rise to poor surface quality and machinability. In addition, inclusions can also induce premature failure in the cast component [8]. With the present-day demands on product integrity, filtering the metal prior to casting has become the norm on most cast-shop floors.

In the production of SiC-particle-reinforced Al–Si–Mg composites, the introduction of the SiC particles into the melt, the need for mechanical stirring to avoid the SiC particles settling or "sedimenting" in the melt, and the recycling of the composite material, makes these composites more susceptible to contamination by inclusions such as oxides, spinel and other harmful metallics. Fluxing treatments, which have

0022–2461

long been applied to cast aluminium alloys (primarily to accelerate inclusion removal as well as to retard oxidation and to clean oxide build-up from the crucible [9–11]), cannot be used to process molten composite material, as these procedures also remove the SiC particles from the melt [12, 13].

Among the large varieties of flux compositions used in cast aluminium alloys, many are based on NaCl–KCl system, with approximately equal amounts of each constituent. It is also reported that fluxes containing sodium salts should not be used with alloys having high (> 2 wt %) levels of magnesium [10]. However, no definite conclusions appear to have been advanced for Al–Si–Mg alloys containing < 1 wt % Mg, and, likewise, there is no literature available for their composites. Purely as an academic exercise, therefore, fluxing was tried on one of the four composites studied in this work to ascertain the consequences for the composition and the related mechanical properties of the composite.

The mechanical properties are known to be determined by the chemical composition of the alloy, the molten-metal processing parameters and the casting method and, finally, the heat treatment applied to the cast product. The heat treatment is one of the more important factors controlling the mechanical properties since it can be used to obtain the optimum combination of strength and ductility for a given alloy system. In general, the three steps involved in any heat treatment are: (i) solutionizing at a temperature close to the eutectic temperature, (ii) quenching, and (iii) subjecting the casting to natural and/or artificial ageing. Variations in each of these steps, reflected by corresponding variations in the mechanical properties can thus be manipulated to derive a particular combination of the strength–ductility required of a specific cast component. While extensive data is available on the heat treatment of Al–Si–Mg alloys [14–18], relatively little is documented for their composites [19, 20].

The present work reviews the results of an extensive study carried out at the Université du Québec à Chicoutimi in Chicoutimi, Québec, by the Industrial Research Chair on the Casting and Solidification of Aluminium group, on different aspects of Al–Si–Mg/SiC(p)-type MMCs. The four composites investigated had matrix alloys containing 7 or 10 wt % Si, reinforced with either 10 or 20 vol % SiC particulates. In particular, the castability and soundness of such composites/castings in terms of the melt fluidity, and the effect of the solidification rate and of inclusions on the mechanical properties were investigated. The effects of employing fluxing procedures similar to those used in Al–Si–Mg alloys on the resulting mechanical properties, and of optimizing the heat-treatment parameters with regard to these properties were also investigated. By examining the microstructural changes occurring during the various stages of processing, the influence of the processing parameters on the mechanical properties was evaluated. The microstructures themselves were monitored by measuring the dendrite arm spacing (DAS), porosity and SiC-particle content and distribution in the castings obtained, as well as the amount of oxide inclusions and other harmful reaction products (like Al_4C_3) also present.

It is appropriate to point out here that, after conducting studies on the fluidity and castability of these composites and the soundness of the castings obtained from them, and finding that the Al–10 wt % Si–Mg/$SiC/10_{(p)}$ composite (named S10 in Table I) gave the best results, further investigations covering other aspects reported here were mostly carried out on this composite, with another composite (or the base alloy) being investigated in some cases for comparison.

2. Experimental procedure

2.1. Materials and melt preparation

The chemical compositions of the four composites studied are given in Table I. The composite materials were received in the form of 12.5 kg ingots from Duralcan Canada, Usine Dubuc, Chicoutimi, Québec. In Table I, the composites are coded A10, S10, A20 and S20, depending on whether the Al–Si–Mg base alloy contains 7 wt % Si (A) or 10 wt % Si (S) and whether it is reinforced with 10 vol % (A10, S10) or 20 vol % (A20, S20) SiC particulates. The Si and SiC contents given correspond to the standard specifications; the actual values can differ from ingot batch to ingot batch, as is observed in Table I. Nonetheless, the composites are still referred to by their standard codes throughout this paper for brevity and convenience. Correctly speaking, however, the currently accepted Aluminum Association (AA) nomenclature for composites is: alloy/reinforcement type/volume $percent_{morphology}$–temper, and the four composites are correctly designated in column 2 of Table I.

TABLE I Chemical composition of the four Al–Si–Mg/$SiC_{(p)}$ composites studied

Composite code	Aluminium Association specification	Chemical composition of the Al–Si–Mg matrix alloy								SiC (vol %)
		Si	Fe	Cu	Mn	Mg	Ti	Ni	Sr	
A10	Al–7Si–Mg/SiC_{10p}	7.45	0.13	0.019	0.003	0.40	0.10	–	0.014	11.30
S10	Al–10Si–Mg/SiC_{10p}	9.46	0.14	0.004	0.003	0.58	0.11	–	0.013	11.34
A20	Al–7Si–Mg/SiC_{20p}	7.17	0.11	0.005	0.004	0.41	0.10	0.004	0.013	18.83
S20	Al–10Si–Mg/SiC_{20p}	9.16	0.15	0.012	0.004	0.62	0.09	0.004	0.013	19.98

The ingots supplied were cut into small pieces (about 76.2 mm^3 ($3 \times 3 \times 3$ in^3)) and heated at 400 °C for at least 2 h prior to remelting in either 7 or 25 kg capacity silicon-carbide crucibles, using an electrical-resistance-heating furnace. During remelting, when the composite was above the mushy zone, the melt was stirred with a graphite impeller specially designed for this purpose. The melting temperature was kept close to 735 ± 5 °C. The castings were made in a Stahl mould (permanent cast-iron mould) to produce test bars for tensile-property measurements. The melt and mould temperatures were varied according to the study being conducted. The pouring temperature was usually very close to 725 °C. Specimens for chemical analysis were also cast simultaneously for each pouring.

Composite-alloy melts cannot be degassed as is customary for the base alloy [12, 13, 19], since this tends to remove the SiC particles, which negates the purpose of the reinforcement. This, the only means of reducing the hydrogen content in these melts is by taking precautionary measures such as preheating and appropriate stirring. Preheating ensures a dry atmosphere for the material, whereas an appropriate stirring speed allows the maintenance of a stable oxide layer on the melt surface which serves to isolate the melt from the atmosphere above it [21]. With these precautions, the hydrogen level in the composite melts could be controlled to within 0.15–0.2 ml per 100 g of aluminium, which was an acceptable value.

2.2. Fluidity-test procedure

Fluidity-test measurements were carried out on all four composites, for melts held at various temperatures ranging from 725 to 850 °C, using a Ragone fluidity tester (supplied by George Fischer Foundry Systems, Inc., Michigan, USA), where the length of solidified tube indicated the corresponding fluidity [22]. Fluidity is measured in terms of the distance a stream of molten metal will flow in a spiral or channel before it stops flowing because of solidification. In the Ragone fluidity tester, the spiral channel is replaced by a tube (a thin-walled stainless steel) bent at one end for the introduction of metal. The pressure head is provided by an adjustable partial vacuum at one end of the .tube. The vacuum (measured by a gauge in mm Hg) can be converted to the effective metal head (in in Hg) using a given standard formula to compare the mould-filling abilities of different metals. This test is sensitive to metal properties and, unlike the spiral test, is independent of the pouring speed [22]. In the present work, in one set of fluidity-test measurements, the melts were heated to 850 °C, cooled down to 725 °C and then tested for their fluidity. In every case, the melt was stirred for about 30 min prior to testing. Specimens for metallographic observations were taken from the central part of the solidified-tube lengths (rods) obtained from these fluidity tests. From the same rods, specimens were also prepared for X-ray analysis, to determine the presence of Al_4C_3, silicon and SiC [23].

2.3. Filtration

Filtration used zirconia-ceramic foam filters and was carried out under gravity and under pressure (porous-disc filtration apparatus (PoDFA) method [24]). Under gravity, ceramic foam filter discs (10 ppi, 50 mm in diameter, 50 mm thick) were placed at the bottom of 380 mm long stainless steel tubes. These tubes were heated at 600 °C before casting. Under pressure, discs (20 and 30 ppi, 25 mm in diameter, 25 mm thick) were placed at the bottom of silicon-carbide crucibles (2.5 kg capacity) with an orifice ($\sim$ 10 mm in diameter) at the bottom, just underneath the filters. They were heated at 650 °C before the liquid composite was transferred to them. Thereafter, they were placed in the pressure chamber of a PoDFA [24] unit and dry air (with a pressure of approximately 0.07 MPa) was used to force the liquid through the filters into the mould. In both cases, the filters were positioned in place using Fiberfrax, a refractory cement.

Test bars obtained from filtration studies (filtered and unfiltered melts of the S10 composite) were tested radiographically to determine their defect levels. All radiography tests were conducted at Alcan International's Kingston R and D Centre, Kingston, Ontario, and the radiographs obtained were compared with standard reference radiographs from ASTM 155, following standard ASTM procedures (see [21] for the details).

2.4. Fluxing

The fluxing process used for foundry aluminium alloys was simulated for the S10 composite, employing Foseco flux Coveral DR908 (45 wt % NaCl, 45 wt% KCl, 10 wt% Ca_2SO_4). Flux doses of 2 and 5 wt% of the total charge were used. For comparison purposes, the unreinforced base alloy was also fluxed, using only a 2 wt % dose. The flux powder was preheated at 400 °C for about 1 h to ensure dryness. After stirring was started and when the temperature of the melt reached $\sim$ 700 °C, the flux powders were evenly scattered over the whole melt surface. Stirring was timed from when the temperature of the flux-covered melt reached 725 °C; the flux agent was also in the liquid state at this temperature [9].

2.5. Solidification rate

To investigate the effect of the solidification rate (in the range 0.1–100 °C s^{-1}) on the dendrite structure and SiC-particle distribution (and related mechanical properties), different moulds were employed, and the mould temperature was varied. The melt was held at 735 ± 5 °C, and the pouring temperature was very close to 725 °C. For mould temperatures in the range 300–450 °C, the molten metal was poured into the central zone of a Stahl mould. At mould temperatures of 25–75 °C, the mould was first preheated at 150 °C, then allowed to cool to the required temperature before casting, the casting was made through side reservoirs using an external riser preheated at 800 °C.

To obtain solidification rates of the order of 0.1 °C s^{-1}, a graphite mould (61 mm wide and 127 mm long) heated at 850 °C before casting and isolated with Fiberfrax insulation to retard the solidification, was used. To achieve solidification rates close to 100 °C s^{-1}, however, a cast-iron mould (41 × 51 mm^2 in cross-section and 71 mm long), with an ingot cavity of 6.1 mm diameter and 41 mm long, was employed. No preheating was applied; that is, the mould was held at room temperature.

In connection with the solidification studies, the effect of the mould temperature on the *castability* of the four composites was investigated, where the mould temperatures were kept at 275, 300, 350, 400 and 450 °C, respectively. From these studies, it was determined that the A composites required a mould temperature of 400–450 °C to produce optimum castings, whereas the S composites could be cast at or below 400 °C [23].

2.6. Heat treatment

Heat-treatment studies were carried out on S10-composite castings. As-cast test bars were subjected to the following T6 heat treatment (recommended by the manufacturer for this composite) [19]:

(i) Solution treatment: 8 h at 538 °C (± 2 °C)
(ii) Quenching: water at 60 °C
(iii) Artificial ageing: 5 h at 155 °C

where treatment involving only steps (i) and (ii) comprises the T4 temper.

2.7. Tensile testing

Tensile tests were performed under uniaxial tensile loading on specimens taken from as-cast or tempered test bars (the specimen dimensions were: 12.5 mm in diameter and 50 mm in gauge length), employing an Instron testing machine equipped with a data-acquisition system that supplied the stress–strain data during testing. All tests were conducted at room temperature at a strain rate of $\sim 4 \times 10^{-4}\ s^{-1}$. Mechanical properties, namely, yield stress (YS) at a 0.2% offset strain, ultimate tensile strength (UTS), and fracture elongation (EL(%)) as well as a plot of stress–strain were derived from the data-acquisition and data-treatment systems. Each reading in the measurements shown in subsequent figures represents an average value taken from two test bars that were simultaneously produced from the same Stahl mould casting.

2.8. Metallography

Metallographic specimens obtained from different sources (as-cast or tempered test bars, solidified tubes obtained from fluidity tests, etc) were polished using a technique specially developed for such composites. Keller's reagent was used to etch the samples, wherever required. The polished specimens were then variously examined for contents of Al_4C_3, porosity, oxide inclusion and SiC and distribution, using an optical microscope (Olympus PMG3). The SiC, porosity and oxide-inclusion volume fractions were measured by means of a Leco 2001 image-analyser system, attached to the optical microscope (for the details see [23]). Dendrite arm spacings (DASs) for these specimens were also measured using the image analyser. The Al_4C_3 content was measured from optical micrographs (× 200 magnification) using a point-count method [25]. The Al_4C_3 contents reported represent averages taken over at least four micrographs for each specimen. Microstructures were observed either by means of the optical microscope or by an S-2700 Hitachi scanning electron microscope, equipped with an energy dispersive X-ray spectrometry (EDX) system.

3. Results

3.1. Remelting conditions

3.1.1. SiC sedimentation

The specific gravity of most of the reinforcements used in aluminium MMCs is usually higher than that of molten aluminium, which leads to settling or "sedimenting" in the melt [26]. In $Al/SiC_{(p)}$ composites, sedimentation of the SiC particles to the bottom of the melt crucible normally occurs during remelting once the melt material reaches the mushy zone. As the temperature of the melt rises, the sedimentation increases with increasing fluidity of the molten material. Also, with settling, the upper regions of the melt become denuded of reinforcement, which can result in large differences in melt viscosity and temperature in different parts of the melt [26]. It has been observed that many reinforcements are not thermodynamically stable in molten aluminium and, in the case of SiC held in the melt for a long time, can react with the aluminium-matrix to form Al_4C_3, which adversely affects the fluidity of the melt. Therefore, it is important that mechanical stirring be commenced as soon as the metal is sufficiently fluid. Prior to that, the melt should be stirred manually, to ensure homogeneous mixing of the SiC particles throughout the crucible. Another factor contributing to SiC sedimentation is the "dead time" between castings, when there is no mechanical stirring. This can be avoided by manual stirring for very short times prior to and after casting.

The variation in SiC-particle volume fraction as a function of holding time is shown in Fig. 1. The SiC content was measured using inductively coupled plasma (ICP) analysis carried out at Alcan International's Arvida R and D Centre, Jonquiére, Québec. Continuous stirring is necessary to avoid SiC sedimentation. The chemical-analysis results showed, however, a slight increase in the SiC volume fraction with increasing holding time, due, probably, to sedimentation occurring during the "dead time", as mentioned previously. Manual stirring during this time was found to be effective in decreasing this tendency. In the recycling procedures specified by Provencher *et al.* [27] for Duralcan-composite-foundry alloys, 2 min hand stirring was recommended before pouring to avoid SiC build-up at the bottom of the crucible. The Duralcan composite-casting guidelines [19] allow for a ± 2% fluctuation in the SiC volume fraction;

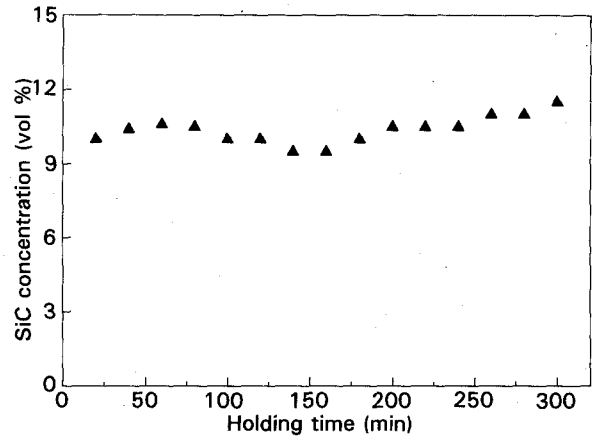

Figure 1 Variation in SiC concentration as a function of the melt holding time.

the $\pm$ 1.5% variation seen in Fig. 1 is within the prescribed limits.

3.1.2. Al_4C_3-fluidity relationship

Under the typical molten-metal processing conditions (that is, high metal temperatures and long processing times) involved in the production of particulate-reinforced composites, the reinforcement particles undergo a reaction at the metal/ceramic interface [28, 29]. In the present work, this reaction resulted in the formation of Al_4C_3:

$$4Al + 3SiC \rightarrow Al_4C_3 + 3Si \quad (1)$$

The kinetics of the reaction depend on the silicon level of the matrix alloy; the level of silicon required to inhibit the reaction is a function of the melt working temperature [28]. Lloyd and Dewing [30] and other workers [31, 32] have studied the Al_4C_3 reaction in detail. Theoretically, silicon levels above 8 at % are required to prevent Al_4C_3 formation. However, practical observations show that the kinetics of the Al_4C_3 formation must also be taken into consideration. From a study of holding times and melt temperatures, it is found that Al_4C_3 forms rapidly at temperatures above 790 and 895 °C in the A and S composite alloys, respectively. The reaction also occurs below these temperatures, but at much lower rates. For the holding times involved in the present studies ($\sim$ 30 min), no significant Al_4C_3 should be formed, except at high temperatures and in composites containing higher volume fractions of SiC [28].

Fig. 2a is an optical micrograph for the A20 alloy (see Table I for its composition) at a melt temperature of 725 °C. The initiation of the Al_4C_3 reaction can be observed at the edges of the SiC particles as indicated by the arrows. As the melt temperature is increased, the reaction proceeds faster; the Al_4C_3 is now clearly visible as black platelets bridging the SiC particles (where the reaction takes place) in Fig. 2b, the microstructure taken from an A20 sample obtained from a melt cooled from 850 to 725 °C.

The Al_4C_3 volume fractions determined for specimens prepared from melts held in the temperature range 725 to 850 °C are displayed in Fig. 3. It is

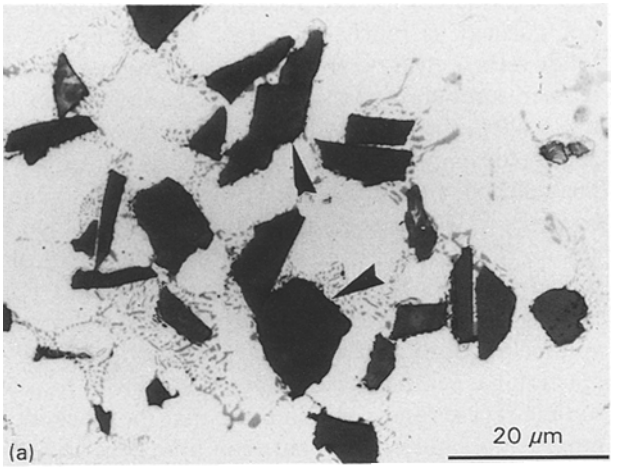

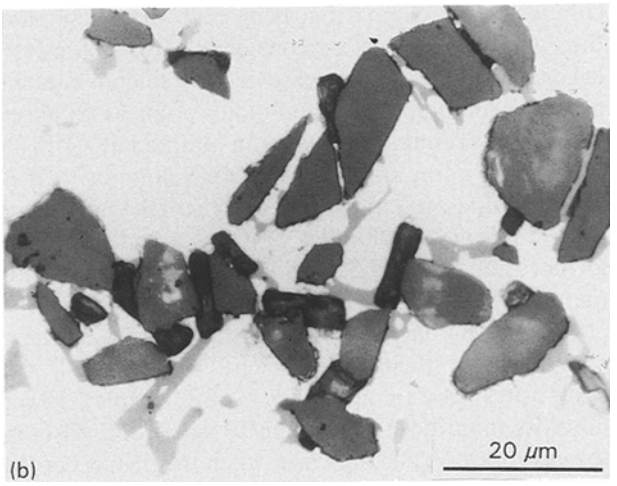

Figure 2 (a) Optical micrograph obtained from an A20 composite sample taken from a melt at 725 °C. The arrows indicate the initiation of the Al_4C_3 reaction at the edges of the SiC particles. (b) Optical micrograph obtained from an A20 composite sample taken from a melt cooled from 850 °C to 725 °C. The Al_4C_3 is clearly visible as black platelets bridging the SiC particles.

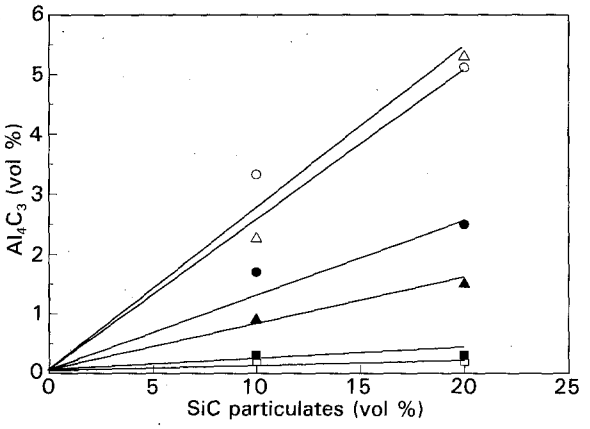

Figure 3 Al_4C_3 volume fractions obtained from fluidity-test specimens for the four composites studied, as a function of their SiC content: (□) A, 725 °C heating; (△) A, 850 °C heating; (○) A, 725 °C cooling; (■) S, 725 °C heating; (▲) S, 850 °C heating; and (●) S, 725 °C cooling.

evident that increasing the silicon content to 10 wt% (that is S composite) results in a significant reduction in the amount of Al_4C_3 phase formed. Increasing the SiC content in the case of A alloys aids in increasing the reaction rate and Al_4C_3 formation (except at

725 °C), whereas for the S composite the reaction is not affected as much. This may be understood as follows: theoretically, ~ 12 at % Si is required at melt temperatures of 850 °C to prevent Al_4C_3 formation. In the A alloy, the level is always much below the value required, even with the additional silicon formed from the reaction. In the S alloy, however, which already contains ~ 10 wt % Si, this value is reached much sooner. This explains the difference in the slopes observed in Fig. 3 for the two composite types. Upon cooling from 850 to 725 °C (which takes over 2 h), the volume fractions increase slightly, suggesting that the reaction has reached its equilibrium state with respect to time. These results also indicate that the reaction is more temperature dependent than time dependent.

Fig. 4 shows the fluidity curves obtained for the four composites. In comparing them, both the silicon and the SiC contents must be considered. It is well established [33] that an increase in the silicon content produces an increase in the fluidity of an Al–Si alloy, with the maximum fluidity being attained at ~ 18 % Si. Thus in going from an A to an S composite, it is expected that an S alloy with a higher silicon content will exhibit greater fluidity. This was found to be true for both the S10 and S20 composites, compared with their A10 and A20 counterparts.

The second factor affecting the fluidity of these composites is their SiC content. From Fig. 4, the composites containing 20 vol % SiC display lower fluidities than those containing 10 vol % SiC. Also, in the case of the A20 composite, when the melt is cooled from 850 to 725 °C, the fluidity is considerably decreased; the metal flow becomes very viscous, to the extent that the melt is nearly frozen at ~ 700 °C, which is well above the melting point of ~ 610 °C for this composite. The dramatic decrease in fluidity is attributed to the formation of a sizeable amount of Al_4C_3, as described previously. X-ray diffraction (XRD) analysis of samples obtained from the fluidity-test measurements (see Section 2.2) showed that increasing amounts of Al_4C_3 form on proceeding from 725 °C to the 850 → 725 °C cooled melt temperature case [23].

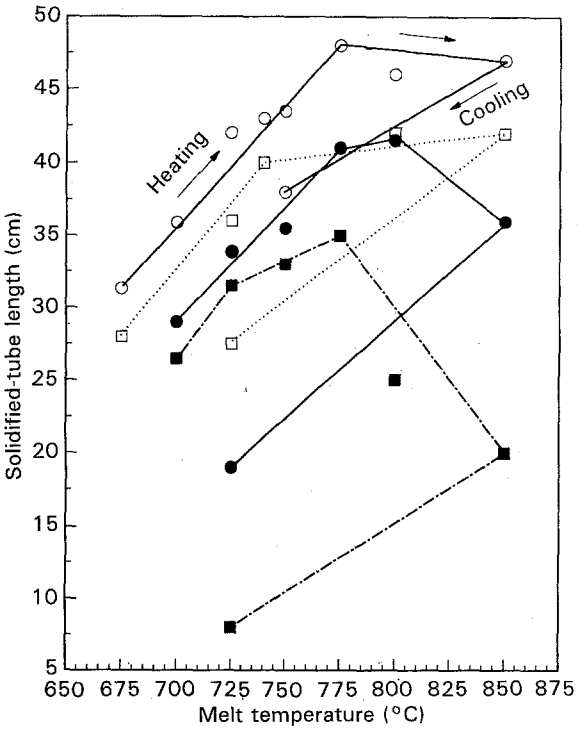

Figure 4 Fluidity curves obtained for the four composite types studied. The arrows (shown for one case only) depict the heating (from 675 to 850 °C) and cooling (from 850 to 725 °C) cycle. (○) S10, (□) A10, (●) S20, and (■) A20.

3.1.3. Spinel formation

In addition to the formation of Al_4C_3 (described in the previous section) $MgAl_2O_4$ and MgO can also be formed, when magnesium is present in the matrix alloy, according to the reactions:

$$3Mg + 4Al_2O_3 \rightarrow 2Al + 3MgAl_2O_4 \quad (2)$$

$$3Mg + Al_2O_3 \rightarrow 2Al + 3MgO \quad (3)$$

the Al_2O_3 is supplied by the oxide-film layer which forms at the melt surface and which can be drawn into the melt at any stage of stirring during the casting process. Wang *et al.* [34] have cited a number of possible chemical reactions that could occur at the metal/ceramic interface during the processing of such composite systems. In the present case, at a melt temperature of 735 °C, the molten alloy is rapidly oxidized at the surface and forms a continuous Al_2O_3 layer that can later be drawn into the melt and thus gain access to the SiC/matrix interface. According to McLeod [35], magnesium levels of only ~ 0.03 wt % are sufficient for spinel formation and it is the stable interface phase observed in AA-6061 and AA-2014 Al-matrix alloys. With 0.4–0.62 wt % Mg in the matrix alloys of the present composites, the stable phase is expected to be $MgAl_2O_4$; it is less likely to be MgO.

Fig. 5 is a scanning electron micrograph taken from an S10 composite sample, showing fine crystals (< 2 μm) that were occasionally observed on the SiC particles. EDX analysis of some of these crystals revealed that in addition to silicon, aluminium and carbon peaks, strong reflections from magnesium were also observed, pointing to the existence of spinel $MgAl_2O_4$ and/or MgO (the aluminium and carbon

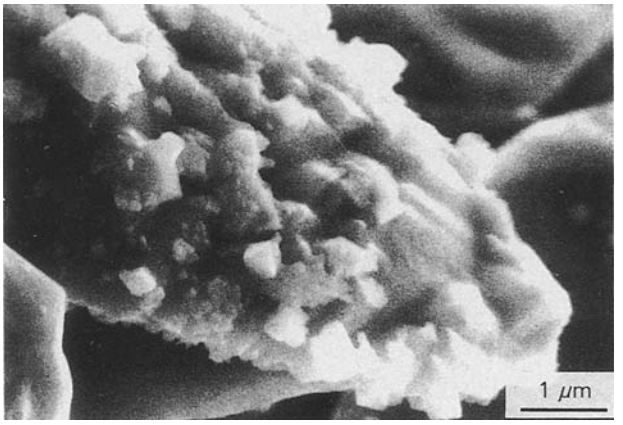

Figure 5 Scanning electron micrograph showing the presence of spinel and/or Al_4C_3 particles in an S10-composite sample cast above 735 °C.

peaks would indicate the possible formation of Al_4C_3). From thermodynamic considerations, as mentioned above, the formation of spinel is more favourable. Wang *et al.* [34] have also demonstrated spinel formation for this composite system at the interface.

In addition to the fine crystals of $MgAl_2O_4$ observed at the SiC/matrix interface, Fig. 5, spinel also occurred in larger form within the composite matrix, exhibiting different morphologies. Various types of spinel are observed; (a) in the form of a thin plate, about 10–15 μm thick and ~ 200 μm long; or (b) in a massive, irregularly-shaped form; or (c) in spherical form, fractured in three (or more) parts [21]. Type c, Fig. 6, was more frequently observed than the other two types.

3.2. Fluxing

Chemical analysis indicated that fluxing–stirring changed the composition of the S10-composite matrix, as well as that of the base alloy, by reducing the magnesium and strontium contents and introducing sodium and potassium, with a considerable magnesium loss being observed in the case of the composite when the flux dose was 5 wt % and the stirring time was 2 h (from ~ 0.56 to ~ 0.07 wt %); the strontium content had a similar response (dropping from ~ 140 to ~ 15 ppm (parts per million)). The volume fraction of SiC particles was also affected (~ 2–3 vol % SiC was lost, due to the removal of the particles by the flux together with the dross).

The effects of fluxing and stirring on the microstructure were mainly reflected by the change in morphology of the eutectic silicon in the fluxed specimens which became much coarser, see Fig. 7b, than in the unfluxed specimens, see Fig. 7a. The eutectic silicon particles in Fig. 7b were recognized as being *under modified* or *insufficiently modified.*

The effect of fluxing and stirring on the ultimate tensile strength (UTS) and the yield strength (YS) of T6-tempered S10 test bars are displayed in Fig. 8. It can be seen that stirring alone did not affect the tensile strength. However, fluxing coupled with stirring reduced the tensile strength of both the composite and the base alloy fluxed with 2 wt % flux, and caused a severe drop in the tensile strength of the composite with a 5 wt % flux addition. Both the loss of magnesium and the presence of Na + K were found to affect the decrease in tensile strength; the former was largely responsible for this, and the latter was responsible to a relatively smaller degree [36].

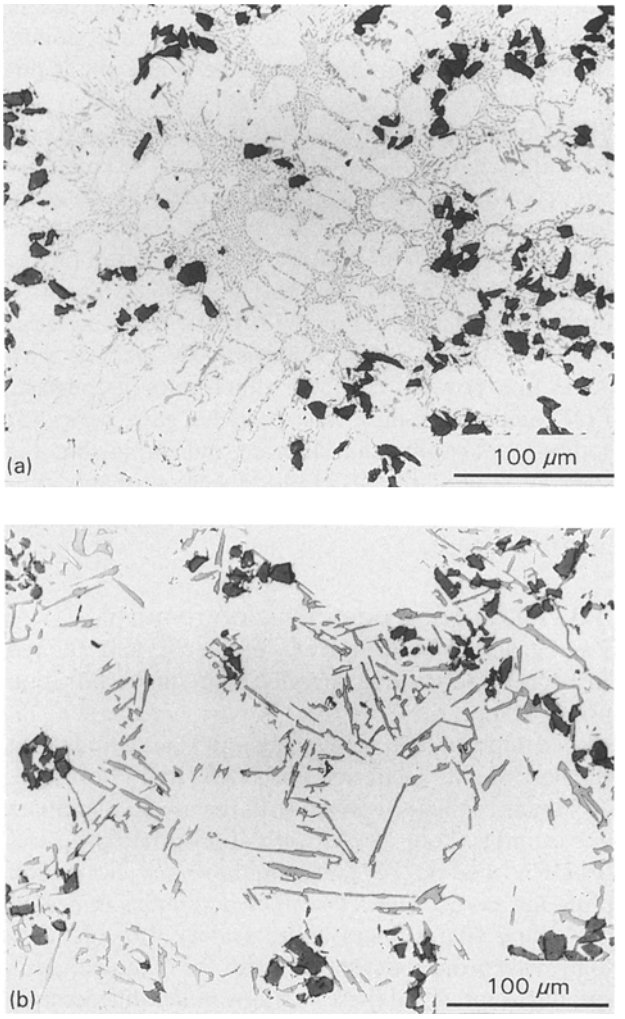

Figure 7 Morphology of eutectic Si in (a) unfluxed and (b) fluxed specimens of the S10 composite.

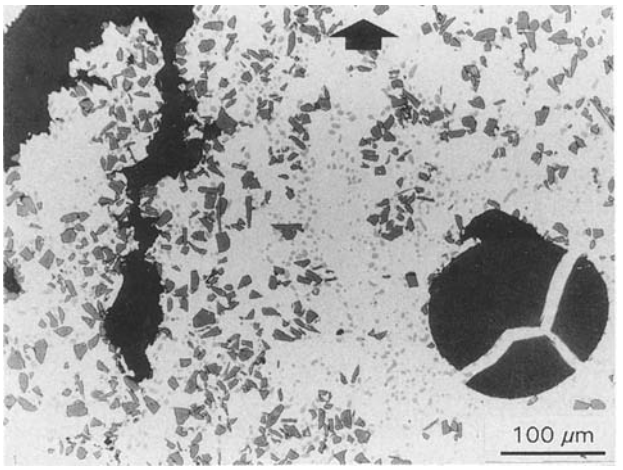

Figure 6 Optical micrograph displaying the fractured spherical form of spinel morphology which is most frequently observed in the composite matrix of S10 specimens.

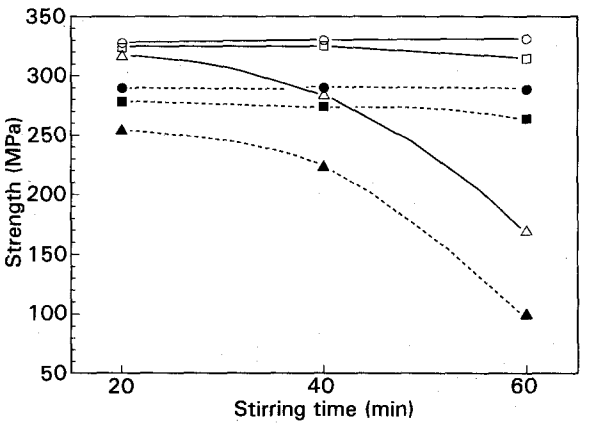

Figure 8 The effect of fluxing and stirring on the tensile properties of T6-tempered S10 composite: (○) UTS, no flux; (●) YS, no flux; (□) UTS, 2 wt % flux; (■) YS, 2 wt % flux; (△) UTS, 5 wt % flux; and (▲) YS, 5 wt % flux.

In all the trials, it was found that under the same fluxing and stirring conditions, sodium and potassium contents in the composite were higher than in the base alloy. The presence of chloride was also detected in the composite. These observations may be accounted for by considering the reaction between the SiC particles and the flux during the fluxing–stirring process. The 10 vol % of particles inside the composite supply quite a large surface area for sodium and potassium adsorption. This adsorption improves their solubilities in the composite by shifting the equilibrium points, though their distribution within the composite is not homogeneous (the concentration is higher at the $SiC_{(p)}$/matrix interface than in SiC-particle-free areas). Also, during fluxing–stirring, the moving SiC particles circulate throughout the melt and hence they have an improved probability of coming into contact with the covering flux. By this contact, flux adsorption on the surface of the SiC particles may occur and this introduces the flux into the melt [36]. The scanning electron micrograph in Fig. 9 shows a SiC particle with some fine powder particles attached to its surface. EDX analysis of these fine particles gave peaks for sodium, potassium and chloride, indicating that the sodium, potassium and chloride were probably present in the form of a salt-phase film at the $SiC_{(p)}$/matrix interface.

3.3. Filtration: oxide inclusion removal

Radiographs obtained from unfiltered and filtered S10-composite casting revealed that simple filtration using 10 ppi filters under gravity adequately removed most of the oxide films, giving castings that showed "slight" inclusion levels (ASTM 155 rating 1, 2), similar to those obtained with the use of finer filters (for example 20 or 30 ppi) with appropriate pressures (PoDFA method [24]). Strength versus elongation plots for as-cast and T6-tempered samples indicated that using 10 ppi filters under gravity was adequate to provide properties that met with the manufacturer's specifications, since there was not much difference in the properties of these samples and the 20 or 30 ppi filtered specimens [21]. The micrographs shown in Figs 10a and b represent typical oxide-inclusion contents observed in samples obtained from unfiltered and filtered castings, respectively.

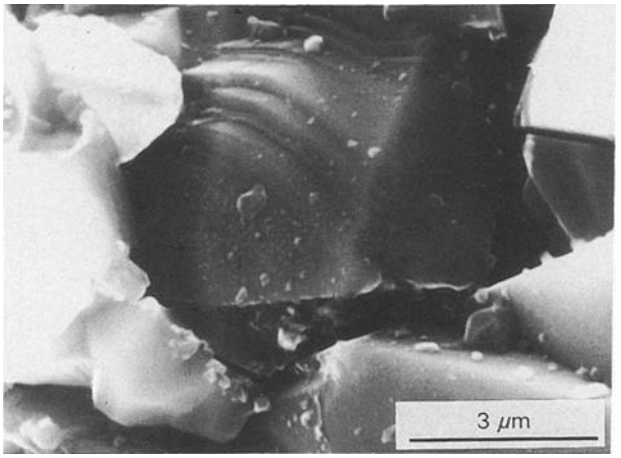

Figure 9 Scanning electron micrograph taken from the fracture surface of a T6-tempered S10-composite specimen, showing flux-powder particles attached to SiC particles.

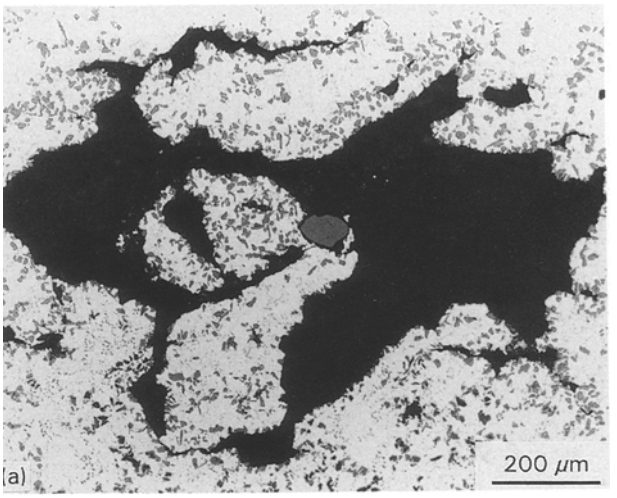

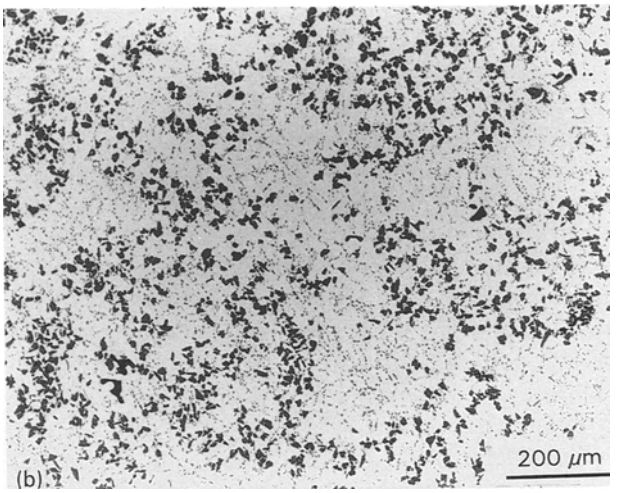

Figure 10 Optical micrographs showing typical oxide-inclusion contents of S10-composite samples: (a) unfiltered and (b) filtered (10 ppi).

In order to quantify the effect of the volume fraction of oxide inclusions upon the tensile properties, specimens were cut close to the fracture surface of the test bars and prepared for metallographic observation and image analysis. For comparison purposes, a specimen prepared from one of the radiography tests was used as a standard to represent clean material. This standard exhibited a porosity volume fraction of $\sim 0.1\%$, see Fig. 10b.

The volume fraction of oxide inclusions was measured by scanning the complete specimen surface area for these inclusions, using an optical microscope in conjunction with an image analyser. Quantification (bulk evaluation) by image analysis was carried out in the manner usually employed for volume-fraction measurements of any specified phase [23]. It should be mentioned that other methods of measuring the oxide-inclusion content also exist; for example, the method employed at the Arvida R and D Centre, Alcan International Limited, Jonquière, where the concentration of oxide films (that is, oxide inclusions observed in the form of thin, ravelled or lumped films) in determined from the relation:

$$x = N(L_{av} + L_{max})$$

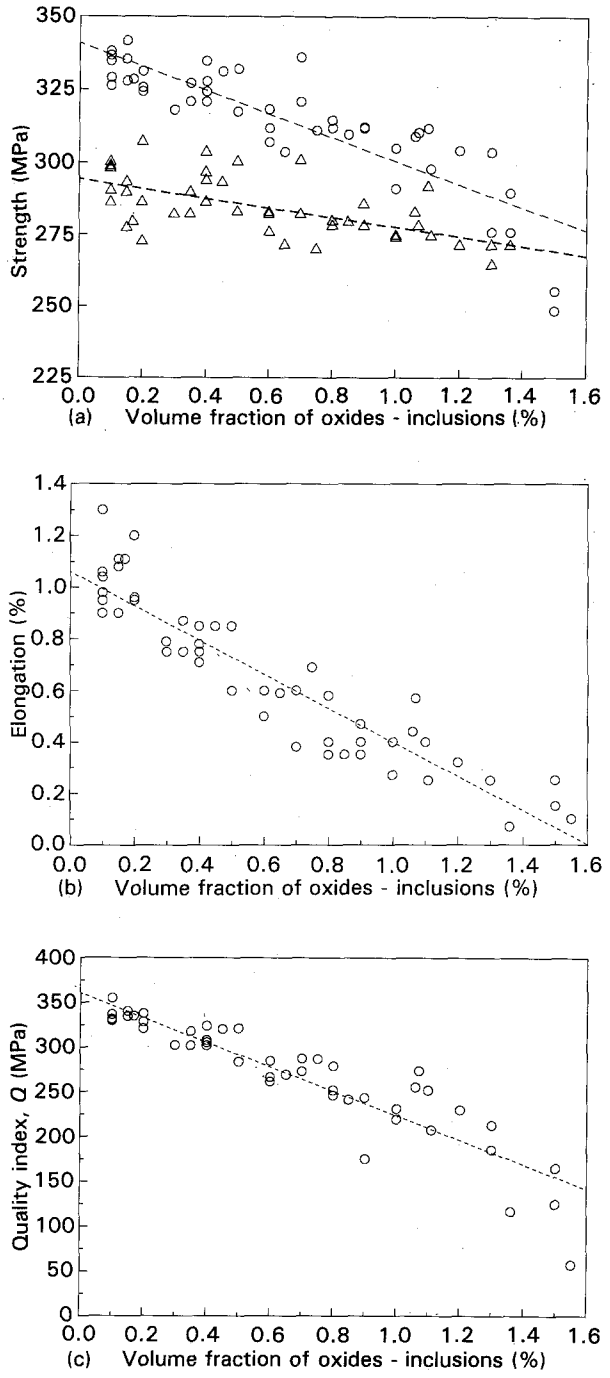

Figure 11 Variations as a function of the oxide-inclusion content in S10 composite of: (a) (○) UTS and (△) YS, (b) elongation, and (c) quality index.

where x is the concentration of the oxide film (mm cm^{-2}) with L_{av} and L_{max} representing the average and maximum lengths of oxide film in millimetres, and N representing the total number of oxide films found within a square centimetre [27].

Fig. 11 shows the variation with the oxide inclusion content of the tensile properties of S10 composites. The readings represent single test-bar-specimen measurements in each case, and were obtained from test bars subjected to a T6 treatment. In Fig. 11a, the scatter in the values for both UTS and YS is about $\pm$ 10.3 MPa. Taking the dashed lines (obtained by the least squares method) to represent linear relations between the UTS or the YS and the oxide-inclusion content, the relationships can be expressed as:

$$\text{UTS} = 340.77 - 40.24x \quad (4)$$

$$\text{YS} = 294.43 - 16.81x \quad (5)$$

where x represents the volume fraction of oxide inclusions. Apparently, a similar correlation between the oxide-film (inclusion) concentration and the UTS was obtained by Provencher *et al.* [27] for an Al–Si–Mg/$SiC_{(p)}$-composite alloy containing 7 wt % Si and 15 vol % SiC particles. Strictly speaking, however, a more detailed comparison cannot be made, since both the composite alloy studied as well as the method of determining the oxide concentration were different in that study to those used in this study.

The plots of the elongation, Fig. 11b, and the quality index (Q = UTS (MPa) + 150 log EL), Fig. 11c, also show a linear relationship. Again, from the least squares method, these relations may be written as:

$$\text{EL} = 1.06 - 0.66x \quad (6)$$

$$Q = 360.22 - 136.64x \quad (7)$$

3.4. Effect of the solidification rate

The dependence of the dendrite arm spacing (DAS) on the solidification rate (related to the mould temperature) for the four composites is shown in Table II, where *edge* and *centre* refer to DAS readings taken from the edge or the central region, respectively, of the specimen cross-section. The DAS is related to the solidification rate by the expression:

$$d = Ar^{-n} \quad (8)$$

where d is the DAS in micrometres, r is the solidification rate (°C s^{-1}), A is a constant and n has values of 0.33 and 0.334 for the A and S composites, respectively. From Equation 8 and from measurements of the DASs of samples obtained from different mould temperatures, the estimated solidification rate for the 25–75 °C mould temperature lies in the range 60–40 °C s^{-1}, and in the ranges 20–25 °C s^{-1} and 8–10 °C s^{-1} for the 300 °C and 450 °C mould temperature, respectively.

Fig. 12 depicts the microstructures taken from the central regions of S10 specimens obtained from mould temperatures of 50 °C ($\sim$ 50 °C s^{-1}) and 450 °C ($\sim$ 10 °C s^{-1}). It can be seen that refinement of the microstructure by increasing the solidification rate brings about a more uniform SiC-particle distribution, whereas lowering the solidification rate leads to clustering of the SiC particles in the interdendritic regions.

Fig. 13 shows the strength parameters, UTS and YS, for A10- and S10-composite samples obtained from melts that were cast after 20, 40 and 60 min stirring time. A significant dependence of these parameters on the DAS up to 18 μm is observed, after which the properties stabilize for higher values of the DAS (up to the 23 μm maximum value observed in the present measurements).

TABLE II Variation in the average dendrite arm spacing (DAS) with mould temperature and solidification rate for the four composites studied

Composite	Average DAS (μm)					
	Mould temperature, 75 °C; SR,[a] ~ 40 °C s^{-1}		Mould temperature, 300 °C; SR,[a] ~ 22.5 °C s^{-1}		Mould temperature, 450 °C; SR,[a] ~ 10 °C s^{-1}	
	Centre	Edge	Centre	Edge	Centre	Edge
A10	13.91	11.45	20.84	15.34	24.64	20.23
S10	11.09	9.55	16.75	13.91	22.73	18.59
A20	–	–	11.54	13.05	13.24	16.54
S20	–	–	10.13	12.03	12.50	16.90

[a] SR, solidification rate

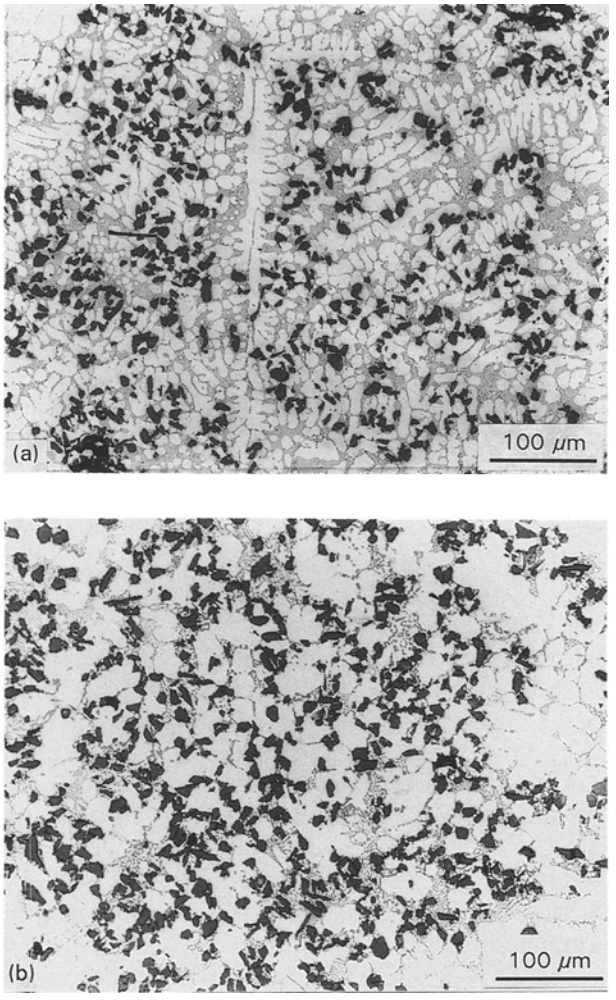

Figure 12 Optical micrographs taken from the central region of the specimen cross-section of S10-composite samples obtained at mould temperatures of: (a) 50 °C, and (b) 450 °C.

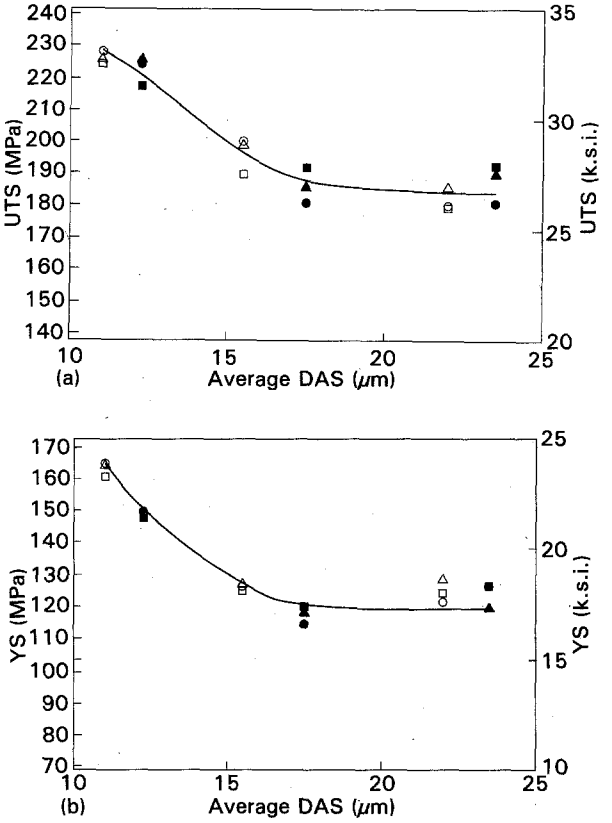

Figure 13 Variation in tensile properties (a) UTS and (b) YS with average DAS for the following stirring times: (○) S10, 20 min; (△) S10, 40 min; (□) S10, 60 min; (●) A10, 20 min; (▲) A10, 40 min; and (■) A10, 60 min.

From Figs 12 and 13 and Table II, it can be concluded that the as-cast mechanical properties are mainly controlled by the matrix microstructure and SiC-particle distribution, both of which are dependent on the solidification rate. A uniform distribution of SiC particles coupled with a fine DAS are essential to obtain good levels of strength and ductility [37]. The stabilization of the properties with higher values of DAS can be explained in part as resulting from the improvement in casting soundness obtained at mould temperatures close to 400 °C or more [23].

3.5. Heat treatment

Shivkumar *et al.* [15, 17] have reported on the effect of increasing the solution time and temperature on the tensile properties of A356 alloys. Their results show that increasing the solution time at 540 °C for Sr-modified permanent mould castings from 25 to 800 min does not produce significant changes in the elongation or the UTS; however, a noticeable increase in the YS is observed. According to them, increasing the solution temperature from 540 to 550 °C is more efficient at improving the tensile properties: properties observed after 400 min at 540 °C are obtained after only 50 min at 550 °C. Further increases in the solution temperature reduce the tensile properties. Silicon-particle sizes for a solution time of 200 min are 2–4 μm

and 30–40 μm, at solution temperatures of 540 and 570 °C, respectively.

Tensile properties of the S10 samples solution treated at 540 °C in the present study are summarized in Fig. 14. The beneficial effect of increasing the solution time at this temperature appears in the stabilization of the properties. For example, after 4 h, the YS and UTS increase from 124 and 537.4 MPa to 199.8 and 289.4 MPa, respectively, and remain constant thereafter (up to 24 h).

It is found that the elongation (Fig. 14b) is the parameter that is the most sensitive to heat treatment at 540 °C. From the results, it can be seen that optimum values of elongation are obtained after 4 h solution treatment at 540 °C (shorter solution times were not tried). However, hardness measurements showed an improvement in the composite strength after 2 h and there was a trend similar to that seen in Fig. 14a for the tensile strength [38]. Therefore, it is quite possible that the initial improvement in these properties could commence at solution times of 2 h or even less.

The quality index, a parameter that combines the UTS and elongation [39] and is expressed as

$$Q\,(\mathrm{MPa}) = \mathrm{UTS}\,(\mathrm{MPa}) + 150 \log \mathrm{El}(\%) \quad (9)$$

is plotted as a function of the solution time in Fig. 14a. The quality index increases with the solution time because of the continuous dissolution of Mg_2Si and the spheroidization of the silicon particles. Contrary to the work of Meyers [40] and Shivkumar *et al.* [15] on A356 (in which a linear relation between Q and the solution time, t, was reported, with a best fit with $t^{1/3}$), the present composite, after 4 h solution time at 540 °C, showed no further variation in Q with time up to 24 h.

As mentioned previously, the recommended heat treatment for S10 composites is T6 [19]. The results of Tsukuda *et al.* [41] and Shivkumar *et al.* [16] on the tensile properties of aged A356 alloys indicate that both the YS and the UTS increase with ageing time and temperature, while the elongation and impact show an opposite trend. Ageing at temperatures higher than 155 °C ensures good strength, whereas high elongation and impact strength are obtained at lower temperatures.

Fig. 15a shows the variation in YS, UTS and Q and for T6-treated samples as a function of the initial solution time. A rapid increase in all three parameters is seen after solution treatment at 540 °C for 4 h. After 8 h at 540 °C (the recommended treatment), the tensile strength parameters remain stable; that is, a further increase in the solution time has no significant effect on the T6 tensile properties. Elongation, however, exhibits an opposite trend, Fig. 15b. In spite of this, the Q values still remain close to the UTS values and are only slightly affected by the decrease in elongation, which is typical of hard/brittle materials.

From the hardness (Rockwell E) and tensile-property measurements (YS, UTS) of T6 specimens aged

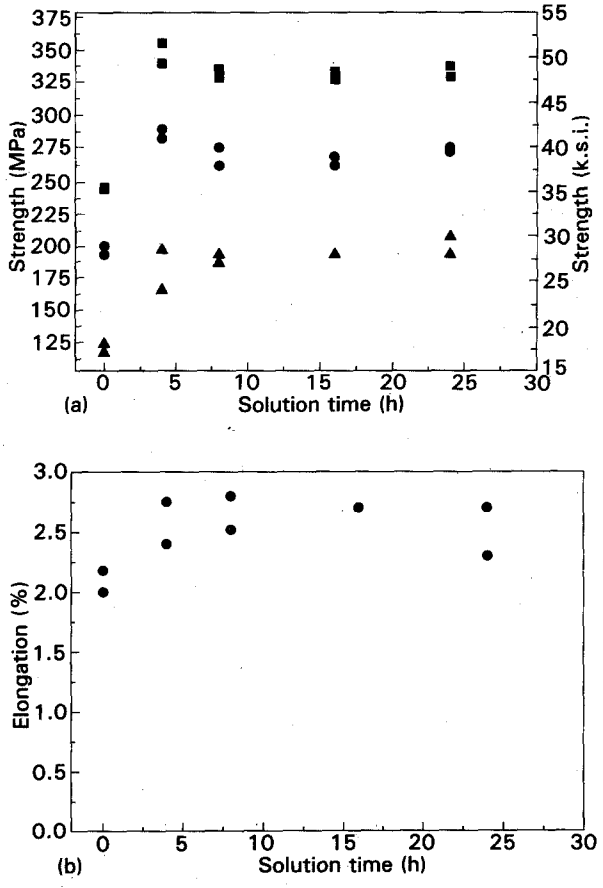

Figure 14 Variation, as function of solution time for T4-treated S10-composite specimens, of: (a) (●) UTS, (▲) YS, and (■) the quality index, Q; and (b) elongation.

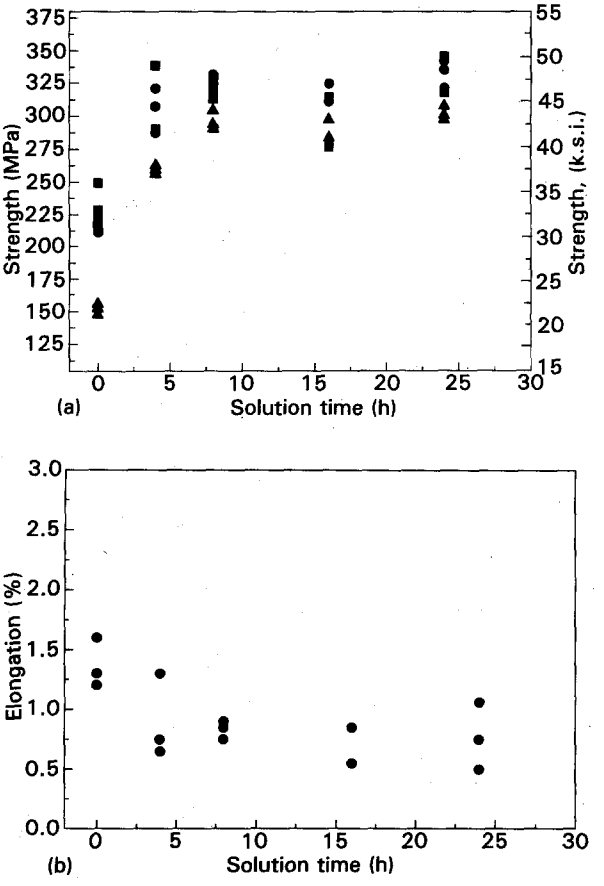

Figure 15 Variation, as function of solution time for T6-treated S10-composite specimens, of: (a) (▲) YS, (●) UTS, and (■) the quality index, Q; and (b) elongation.

directly or pre-aged at room temperature for 24 h prior ageing [38], it was determined that the recommended ageing time fell in the under-aged region. The primary purpose of ageing is to bring about precipitation of the fine-scaled Mg_2Si particles, which strengthen the alloy. Interestingly, strengthening due to Mg_2Si precipitation is solution-temperature dependent rather than solution-time dependent, as is evidenced by Fig. 16, where the hardness behaviours of T4-treated and T6-treated samples are separated by a certain gap. That is to say, the composite-alloy strength in the T6 condition is strongly related to the previous T4 strength. In a heat-treatment study of the mechanical properties of an A356/SiC/20$_{(p)}$ composite, Hammond also reported that the solution time has no significant effect upon the average tensile properties; the ageing time, however, does have a significant effect [20].

3.6. Porosity formation

In the context of the subject matter of this paper, it is important to touch upon the topic of porosity formation in these composites. Porosity, as is well known, is one of the biggest problems in the production of premium-quality aluminium castings; it is always a case for concern because, in addition to affecting the surface finish, its presence can be detrimental to the mechanical properties and corrosion resistance of the casting [42].

In an Al/SiC$_{(p)}$ composite, the occurrence of porosity can be attributed variously to the amount of hydrogen gas present in the melt, the oxide films formed at the surface of the melt which can be drawn into it at any stage of the stirring, the presence of inclusions in the melt, as well as incorrect feeding or shrinkage that can arise from an incorrect mould temperature. Porosity levels, needless to say, must be kept to a minimum in order to produce sound castings with optimum properties.

In the course of our studies on the four composites, porosity formation was also studied simultaneously [23, 43, 44]. In the present context, however, these results are best represented by Fig. 17, which shows the average void volume content (vol %) in A20 and S20 composite samples obtained at different mould temperatures. The void-volume (porosity-volume) fractions were measured by image analysis at $\times 200$ magnification. It can be seen that the S composite has a much lower void-volume fraction than the A composite. Also, increasing the mould temperature improves the soundness of the casting as reflected by the decrease in the porosity level. In addition, the much steeper slope for the A composite, on proceeding from a mould temperature of 300 to 450 °C indicates that the S alloy gives a much better overall soundness.

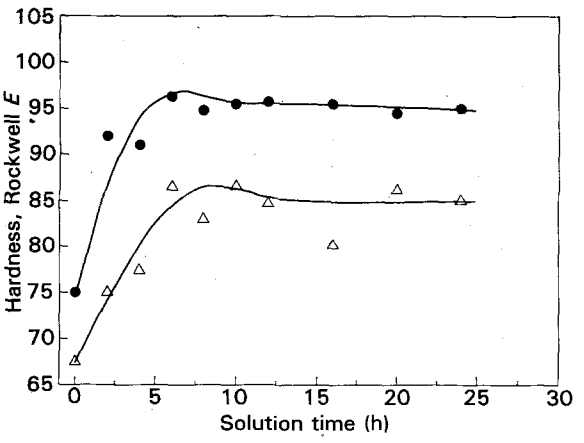

Figure 16 Variation in hardness (Rockwell *E*) as a function of solution time for (△) T4-treated and (●) T6-treated S10-composite specimens.

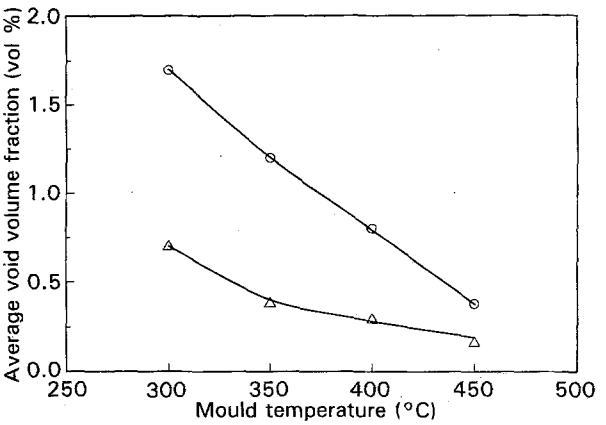

Figure 17 Void-volume fractions, obtained at different mould temperatures, for: (○) A20, and (△) S20 composite specimens.

It was also found, in general, that while the porosity level in clean melts could be maintained below ~ 0.2 %, in oxide-contaminated melts, the level could rise to as much as ~ 0.6 % for a mould temperature of 300 °C and a stirring time of 180 min [43].

4. Conclusions

1. Continuous stirring of the melt – mechanically and manually – is necessary to avoid sedimentation of the SiC particles, which can result in large differences in melt viscosity and temperature in different parts of the melt and can lead to the unwanted formation of Al_4C_3, whose presence is severely detrimental to the fluidity, the reinforcement, and the mechanical properties.

2. A low silicon content coupled with a high SiC level accelerates the formation of Al_4C_3 (about 6 vol % at 850 °C), which is detrimental to the fluidity and hence castability of the composite alloy. Increasing the silicon content from 7 to 10 wt % leads to a significant reduction in the amount of Al_4C_3 (about 2 vol %), even with a 20 vol % SiC content.

3. The main types of inclusions observed are Al_2O_3 (in the form of films) and spinel or $MgAl_2O_4$ which can occur either at the SiC/matrix interface (as very fine (< 2 μm) crystals) or within the matrix in much larger form, with different morphologies.

4. Fluxing changes the chemical composition of the composite matrix by removing the alloying elements magnesium and strontium from the melt and by introducing sodium and potassium into the melt. The removal of magnesium softens the composite matrix by reducing the amount of the Mg_2Si-phase precipitate after T6 treatment. This results in a significant

degradation in the mechanical properties of the composite. The presence of sodium and potassium reduces the tensile properties of the composite to a small extent by weakening the cohesion between the SiC particles and the matrix. Therefore, flux treatment using alkali chlorides cannot be applied to $SiC_{(p)}$/Al composites containing magnesium and/or strontium in their matrix.

5. Removal of inclusions by filtration produces a consistent improvement in strength and ductility of the composite. Simple filtration using 10 ppi filters under gravity appears to be adequate, and it compares well with the results obtained using 20 and 30 ppi filters under pressure (PoDFA). Linear regression equations are obtained for the tensile strength, yield strength, elongation and quality index plotted against the volume fraction of oxide inclusions. The presence of an excessive amount of oxide inclusions ($\sim$ 1.4 vol %) lowers the ductility to about 0.15 %, whereas for an oxide volume fraction of 0.1 %, the ductility improves to almost 1.15 %.

6. The as-cast properties of SiC-particulate-reinforced Al–Si–Mg composites are essentially controlled by the solidification rate. Higher rates promote homogeneous distribution of SiC particles which result in higher strength parameters.

7. For the composite samples solution treated at 540 °C, the beneficial effect of increasing the solution time at this temperature appears in the stabilization of the tensile properties. Compared to the matrix alloy, the presence of 10 vol % of SiC in the composite alloy attributes significantly to its strength. Elongation is the parameter found to be most sensitive to heat treatment. Optimum values of elongation may be achieved for solution treatment at 540 °C, and for solution times of 4 h or even less.

8. For the composite alloy, no specific relationship between the quality index, Q, and the solution time, t, was obtained (cf. the linear relationship $Q \propto t^{1/3}$ obtained for the A356 alloy). Direct ageing is recommended for such composites (S10 type). It is found that strengthening due to Mg_2Si precipitation is solution-temperature rather than solution-time dependent.

Acknowledgements

The authors would like to thank Duralcan Canada, Usine Dubuc, Chicoutimi, Québec for supplying the composite materials. The financial support received from the Natural Sciences and Engineering Research Council of Canada, the Fondation Sagamie de l'Université du Québec à Chicoutimi and the Société d'électrolyse et de chimie Alcan (SECAL) is gratefully acknowledged.

References

1. E. J. PETERS, "Ceramic fibre usage in automotive composites", 3rd IAVD Congress, Geneva, March 1986.
2. Dural Aluminum Composite Corporation, Brochure of Products, San Diego, California (1990).
3. P. K. ROHATGI, R. ASTHANA and F. YARANDI, "Solidification of metal matrix composites", edited by P. Rohatgi (The Minerals, Metals and Materials Society, Warrendale, PA, 1990) p. 51.
4. S. A. LEVY, *AFS Trans.* **93** (1985) 889.
5. D. V. NEFF, SDCE The Society of Die Casting Engineers, Inc., 14th International Die Casting Congress and Exposition, 11–14 May 1987, Toronto, Ontario, Canada, paper no. G-T87-034, pp. 1–6.
6. F. FRISVOLD, T. A. ENGH and E. BATHEN, *Light Metals* (1990) 805.
7. S. STROBL, *Modern Casting* **83** (April 1992) 42.
8. D. APELINA and K. K. CHOI, "Foundry processes: their chemistry and physics", edited by S. Katz and F. Landefeld (Plenum Press, New York, 1988) pp. 467–93.
9. D. V. NEFF, "Metals Handbook", 10th Edn, Vol. 2 (American Society for Metals, Metals Park, OH, 1990) pp. 445–96.
10. J. E. GRUZLESKI and B. M. CLOSSET, "The treatment of liquid aluminum-silicon alloys" (American Foundrymen's Society Inc., Des Plaines, IL, 1990) pp. 201–12.
11. P. N. CREPEAU, M. L. FRENYES and J. L. JEANNERET, *Modern Casting* **82** (July 1992) 28.
12. R. E. CARITY, *AFS Trans.* **97** (1989) 743.
13. P. M. BRALOWER, *Modern Casting* **79** (August 1989) 32.
14. D. APELIAN, S. SHIVKUMAR and G. SIGWORTH, *AFS Trans.* **97** (1989) 727.
15. S. SHIVKUMAR, S. RICCI Jr, B. STEENHOFF, D. APELIAN and G. SIGWORTH, *AFS Trans*, **97** (1989) 791.
16. S. SHIVKUMAR, C. KELLER and D. APELIAN, *ibid.* **98** (1990) 905.
17. S. SHIVKUMAR, S. RICCI Jr and D. APELIAN, *ibid.* **98** (1990) 913.
18. S. SHIVKUMAR, S. RICCI Jr and D. APELIAN, "Production and electrolysis of light metals" (Pergamon Press, New York, 1990) pp. 173–82.
19. Duralcan Composite Casting Guidelines, Duralcan USA, San Diego (1990) VIII-1.
20. D. E. HAMMOND, *AFS Trans.* **97** (1989) 887.
21. F. H. SAMUEL, H. LIU and A. M. SAMUEL, *Met. Trans. A* **24A** (1993) 1631.
22. Instructions for No. 4210 Ragone Fluidity Tester, George Fischer Foundry Systems, Inc., Michigan, USA, January (1989) pp. 2–3.
23. A. M. SAMUEL, H. LIU and F. H. SAMUEL, *Compos. Sci. Technol.* **49** (1993) in press.
24. D. DOUTRE, B. GARIÉPY, J-P. MARTIN and G. DUBÉ, *Light Metals* (1985) 1179.
25. E. E. UNDERWOOD, "Metals Handbook", 8th Edn, Vol. 8 (American Society for Metals, Metals Park, OH, 1973) pp. 37–47.
26. D. J. LLOYD, "High performance composites for the 1990's, edited by S. K. Das, C. P. Ballard and F. Marikar (The Minerals, Metals and Materials Society, Warrendale, PA, 1991) pp. 33–45.
27. R. PROVENCHER, G. RIVERIN and C. CELIK, Proceedings of the International Symposium on Advances in Production and Fabrication of Light Metals and Metal Matrix Composites, edited by M. M. Avedesian, L. J. Larouche and J. Masounave (The Canadian Institute of Mining, Metallurgy and Petroleum, Montreal, 1992) pp. 589–604.
28. D. J. LLOYD, *Compos. Sci. Technol.* **35** (1989) 159.
29. D. J. LLOYD, H. P. LAGACÉ and A. D. McLEOD, "Controlled interphases in composite materials", Proc. ICCI-III, edited by H. Ishida (Elsevier, London, 1990) pp. 359–76.
30. D. J. LLOYD and E. DEWING, Proceedings of the International Symposium on Advanced Structural Materials, edited by D. S. Wilkinson (Pergamon Press, New York, 1988) p. 71.
31. T. A. CHERNYSHOVA and A. V. REBROV, *J. Less-Common Metals* **117** (1980) 203.
32. W. C. MOSHIER, J. S. AHEARN and D. C. COOKE, *J. Mater. Sci* **22** (1987) 115.
33. F. R. MOLLARD, M. C. FLEMINGS and E. F. NIYAMA, *AFS Trans.* **95** (1987) 647.
34. N. WANG, Z. WANG and G. C. WEATHERLY, *Met Trans. A* **23A** (1992) 1423.
35. A. D. McLEOD, Proceedings of the American Society for Metals International Conference on the Fabrication of Particulate Reinforced Metal Composites, Montreal, American Society for Metals, Metals Park, OH, 1990, 16–19 September, pp. 25–29.

36. H. LIU and F. H. SAMUEL, *AFS Trans.* **101** (1993) in press.
37. A. LABIB, H. LIU and F. H. SAMUEL, *Mater. Sci. Engng. A* **A160** (1993) 81.
38. F. H. SAMUEL, A. M. SAMUEL and H. LIU, *AFS Trans.* **101** (1993).
39. M. DROUZY, S. JACOB and M. RICHARD, *Fonderie*, **335** (1976) 139.
40. C. W. MEYERS, *AFS Trans.* **93** (1985) 741.
41. M. TSUKUDA, S. KOIKE and M. HARADI, *J. Jpn. Inst. Light Metals* **28** (1978) 8.
42. A. M. SAMUEL and F. H. SAMUEL, *AFS Trans.* **100** (1992) 657.
43. A. LABIB, H. LIU and F. H. SAMUEL, *ibid.* **100** (1992) 1033.
44. A. M. SAMUEL and F. H. SAMUEL, *Met. Trans.* **A 24** (1993) 1857.

Received 11 March
and accepted 3 June 1993